Analyst

Accepted Manuscript

This article can be cited before page numbers have been issued, to do this please use: H. Wang, X. Zhao, H. Yang, L. Cao, W. Deng, Y. Tan and Q. Xie, *Analyst*, 2020, DOI: 10.1039/C9AN02392E.

View Article Online
DOI: 10.1039/C9AN02392E

ARTICLE

Three-dimensional macroporous gold superior to conventional gold disk electrode in the construction of electrochemical immunobiosensor for *Staphylococcus aureus* detection†

Received 00th January 20xx,
Accepted 00th January 20xx

DOI: 10.1039/x0xx00000x

Hui Wang, Xiao Zhao, Hui Yang, Lin Cao, Wenfang Deng, Yueming Tan*, and Qingji Xie

Herein, three-dimensional macroporous gold (3DMG) electrode is demonstrated to be a better choice than conventional gold disk electrode in the construction of an electrochemical immunobiosensor for *Staphylococcus aureus* (*S. aureus*) detection. The 3DMG electrode was prepared on a gold disk electrode by one-step electrodeposition using hydrogen bubbles as dynamic templates. The 3DMG electrode has a high electrochemically active surface area with pore sizes ranging from 20 to 50 μm, and these unique features are conducive to the immobilization of primary antibodies and the capture of *S. aureus*. Secondary antibody (Ab_2) and alkaline phosphatase (ALP) were immobilized on mesoporous silica nanospheres (MSNs), and the resulting ALP-MSNs-Ab_2 composites were utilized as signal tags to construct a sandwich-type electrochemical immunobiosensor. *S. aureus* was measured based on the alkaline phosphatase-catalyzed silver deposition and differential pulse voltammetric detection. The linear range is from 5 to 10^9 CFU mL^{-1}, and the detection limit is 2 CFU mL^{-1} for *S. aureus* detection. Due to the signal amplification of 3DMG electrode, the sensitivity of the immunobiosensor constructing on the 3DMG electrode is 9 times that of an immunobiosensor constructing on a gold disc electrode. The proposed biosensor was successfully applied for detecting *S. aureus* in milk samples.

1. Introduction

The detection of foodborne pathogenic bacteria is important for clinical diagnostics, disease control, environmental testing and food safety, in particular due to the increasing global health issue of increasing antimicrobial resistance.[1] Conventional method for detecting foodborne pathogenic bacteria is based on enumerating and isolating viable bacterial cells in food, and usually involves complicated steps, so conventional bacterial testing method is time-consuming.[2] Due to the development in the field of immunology and molecular biology, many new detection technologies have been developed for detecting foodborne pathogenic bacteria, such as polymerase chain reaction technologies, DNA sequencing technologies, enzyme-linked immunosorbent assay, and ATP bioluminescence.[3-6] These detection methods show great improvement in detection efficiency, but there are some disadvantages including high technical requirements and high cost. Biosensors that make use of antibody and aptamer as the recognition elements have also been used for detecting foodborne pathogenic bacteria.[7-11] Among them, electrochemical biosensors have been recognized as a powerful tool for detecting foodborne pathogenic bacteria, owing to their advantages of fast response, simple operation, low cost, intuitive output, and ease of miniaturization.[12-14] However, the sensitivities of most electrochemical biosensors are still not up to the application requirements, since foodborne pathogenic bacteria usually exist in real samples in very low numbers (<20 CFU mL^{-1}).[15] Therefore, developing an efficient signal amplification strategy is of great importance for improving the sensitivities of electrochemical biosensors.

Three-dimensional macroporous electrodes have been widely used in lithium ion batteries,[16, 17] solar cells,[18] supercapacitors,[19, 20] electrocatalysis,[21-25] catalysis,[26] microbial fuel cells,[27-29] enzymatic biofuel cells,[30] and electrochemical biosensors,[31-33] because of their advantages including large specific surface areas, uniform pores and high electrical conductivity. For instance, three-dimensional macroporous carbon-based electrodes have been explored as anodes in microbial fuel cells to improve the power densities, because the three-dimensional macroporous structures are beneficial to bacterial attachment, electron transfer, and mass transport.[27-29] Despite the fact that three-dimensional macroporous electrodes are beneficial to the immobilization of bacterial cells, three-dimensional macroporous electrodes have scarcely been reported to construct of electrochemical immunobiosensors for detecting foodborne pathogenic bacteria.

In this work, three-dimensional macroporous gold (3DMG) electrode was prepared by one-step electrodeposition on a gold disk electrode using hydrogen bubbles as dynamic templates, and the as-prepared 3DMG electrode was used for the immobilization of primary antibodies (Ab_1) and the capture of *Staphylococcus aureus*

Key Laboratory of Chemical Biology and Traditional Chinese Medicine Research (Ministry of Education of China), College of Chemistry and Chemical Engineering, Hunan Normal University, Changsha 410081, China.
E-mail: E-mail: tanyueming0813@hunnu.edu.cn.

† Electronic supplementary information (ESI) available: Additional experimental section, figures and tables. See DOI: 10.1039/x0xx00000x

View Article Online
DOI: 10.1039/C9AN02393B

(*S. aureus*). Mesoporous silica nanospheres (MSNs) were used for the immobilization of secondary antibody (Ab_2) and alkaline phosphatase (ALP), and the ALP-MSNs-Ab_2 composites were labeled to the captured *S. aureus* cells. Based on the alkaline phosphatase-catalyzed silver deposition and differential pulse voltammetric detection, the biosensor can detect *S. aureus* down to 2 CFU mL^{-1}. Compared with an immunobiosensor constructing on a gold disc electrode, the sensitivity of the immunobiosensor constructing on the 3DMG electrode was greatly improved, highlighting the signal amplification effect of 3DMG electrode.

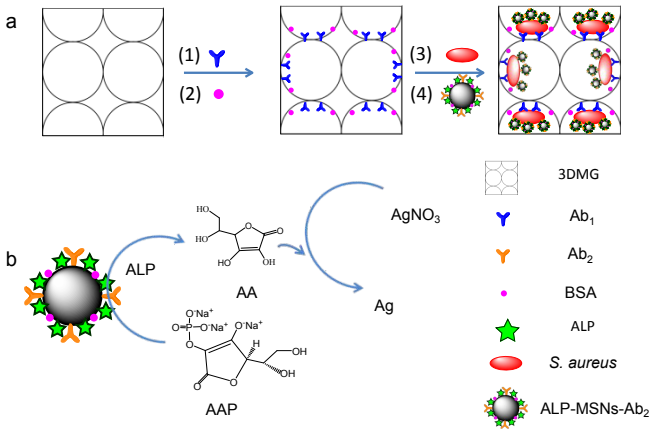

Scheme 1 (a) Illustration of fabrication steps of the 3DMG-based immunobiosensor for *S. aureus* detection. (b) Illustration of ALP-catalyzed Ag deposition.

2. Experimental

Instrumentation and reagents

Instrumentation and reagents were provided in the Supplementary Information.

Preparation of 3DMG and MSNs

The 3DMG electrode was prepared on a gold disk electrode by one-step electrodeposition using hydrogen bubbles as dynamic templates according to a previous method with slight modifications.[34] Briefly, the electrodeposition was carried out at -4.0 V for 500 s in 10 M H_2SO_4 aqueous solution containing 5 mM $HAuCl_4$.

MSNs were prepared following a reported synthesis strategy.[35] Briefly, 9 mL of ethanol, 15 mL of ether, 5 mL of tetraethyl silicate, and 0.5 mL of $NH_3 \cdot H_2O$ were injected in order in 35 mL of water containing hexadecyltrimethylammonium bromide (14 mg mL^{-1}). The above solution was magnetically stirred for 4 h at 27 °C. The precipitates were centrifuged and washed with water/ethanol for 3 times. The resulted products were dried at 60 °C and then calcinated at 550 °C for 4 h to produce MSNs.

Surface modifications of MSNs

For the preparation of amino-functionalized MSNs, 50 mg of MSNs were dispersed in 35 mL of ethanol, followed by adding 0.5 mL of 3-aminopropyltriethoxysilane (APTES). The mixture was magnetically stirred for 24 h at 30 °C. Then the products were separated by centrifugation and dried at 60 °C. The as-prepared amino-functionalized MSNs were used for the immobilization of ALP and Ab_2. 5.0 mg of amino-functionalized MSNs were dispersed in 5 mL of phosphate buffer solution (PBS, pH 7.4) containing N-hydroxysuccinimide (100 mM) and 1-ethyl-3-(3-dimethylaminopropyl)carbodiimide (100 mM), followed by adding 50 μL of 1 mg mL^{-1} Ab_2 and 100 μL of 3 mg mL^{-1} ALP. After shaking for 6 h, the as-prepared ALP-MSNs-Ab_2 composites were centrifuged at 3,000 rpm, and then redispersed in PBS (5 mL) containing 10 mg mL^{-1} bovine serum albumin (BSA). The mixture was agitated for 40 min, and the ALP-MSNs-Ab_2 composites blocked by BSA were centrifuged at 3,000 rpm, redispersed in 5 mL of PBS, and finally stored at 4 °C.

Fabrication and electrochemical characterizations of immunoelectrodes

The fabrication steps of the immunoelectrodes are shown in **Scheme 1a**. To immobilize Ab_1 on the 3DMG electrode, Chitosan (CS) was electrodeposited potentiostatically on the 3DMG electrode at -0.40 V for 100 s in 0.10 M HAc-NaAc buffer (pH 5.1) containing 20 mM H_2O_2 and 0.5 wt.% CS.[36] Then 10 μL of glutaraldehyde aqueous solution (2.5 wt.%) was casted on the CS/3DMG electrode. After reacting for 2 h, the activated CS/3DMG electrode was rinsed with ultrapure water. To immobilize anti-*S. aureus* Ab_1, 10 μL of anti-*S. aureus* Ab_1 (0.1 mg mL^{-1}) was casted on the activated CS/3DMG electrode. After reacting for 12 h at 4 °C, the excess Ab_1 was rinsed with PBS. For blocking the nonspecific binding sites, 10 μL of blocking solution (1 wt.% BSA) was casted on the Ab_1-CS/3DMG electrode and incubated for 1 h at room temperature. After washing with PBS, the BSA/Ab_1-CS/3DMG electrode was incubated with PBS (1 mL) containing a certain concentration of *S. aureus* cells at room temperature for 80 min, where the exact concentration of *S. aureus* was detected by the traditional plate-counting method. After washing with PBS, the obtained *S. aureus*/BSA/Ab_1-CS/3DMG electrode was incubated with PBS (0.2 mL) containing ALP-MSNs-Ab_2 composites (1.0 mg mL^{-1}) for 45 min at room temperature to form ALP-MSNs-Ab_2/*S. aureus*/BSA/Ab_1-CS/3DMG electrode. Finally, the ALP-MSNs-Ab_2/*S. aureus*/BSA/Ab_1-CS/3DMG electrode was washed with PBS.

For comparison, ALP-MSNs-Ab_2/*S. aureus*/BSA/Ab_1-CS/Au electrode was also prepared. The fabrication steps of the ALP-MSNs-Ab_2/*S. aureus*/BSA/Ab_1-CS/Au electrode were similar to those of the ALP-MSNs-Ab_2/*S. aureus*/BSA/Ab_1-CS/3DMG electrode except that the Au disk electrode was used instead of the 3DMG electrode.

Each fabrication step of the immunoelectrodes was characterized by cyclic voltammetry and electrochemical impedance spectroscopy. Cyclic voltammograms (CVs) were recorded at scan rate at 50 mV s^{-1}. Electrochemical impedance spectra were obtained in the frequency range from 1 MHz to 0.01 Hz at voltage amplitude of 5 mV.

Electrochemical detection of *S. aureus*

The immunoelectrodes were subjected to ALP-catalyzed silver deposition (**Scheme 1b**). Briefly, 10 μL of enzymatic reaction solution consisting of 3.5 mM L-ascorbic acid-2-phosphate trisodium salt (AAP), 3.0 mM $AgNO_3$, and 0.07 wt.% $NH_3 \cdot H_2O$ was dropped on the immunoelectrodes. After reacting for 45 min at room temperature, the immunoelectrodes were rinsed with ultrapure water,

and air-dried at room temperature. Then the as-prepared immunoelectrodes were subjected to differential pulse voltammetric detection. The electrodes were placed in a 1 mL of 2 M HNO_3 aqueous solution, and a cathodic potential of -0.3 V was applied for 200 s. Subsequently, differential pulse voltammetric detection was carried out between -0.3 V and 0.7 V, with an amplitude of 50 mV, a pulse width of 50 ms, and a potential step of 4 mV. Differential pulse voltammograms (DPVs) were baseline corrected using the CHI760E baseline-correction command.

3. Results and discussion

Characterizations of 3DMG

The 3DMG were characterized by scanning electron microscopy (SEM). From **Fig. 1a**, one can see that the 3DMG is three-dimensional porous, with pore sizes ranging from 20 to 50 μm. Compared with the sizes of *S. aureus* cells (< 1 μm), the pore sizes of the 3DMG are so large that the diffusion of *S. aureus* cells into the pores of the 3DMG is feasible. The electrochemical behaviors of 3DMG and Au disk electrode were studied in 0.5 M H_2SO_4 aqueous solution. As shown in **Fig. 1b**, the oxidation of Au at both the 3DMG and Au disc electrode starts at ca. 1.1 V, but the shapes of oxidation peaks in the CVs of the two electrodes are distinct, due to the different exposed crystal planes.[37] The cathodic currents near 0 V related to reduction of dissolved oxygen are also distinct in the CVs of the two electrodes, owing to the different oxygen reduction activities of different crystal planes.[38] The electrochemically active surface area (EASA) can be examined by measuring the charge of the reduction peak in the CVs in 0.5 M aqueous H_2SO_4 at 50 mV s^{-1} (**Fig. 1b**), assuming the charge density of 390 μC cm^{-2} during the electroreduction of an oxide monolayer.[39] The EASA of the 3DMG is estimated to be 6.48 cm^2, and the roughness factor (R_f) of the 3DMG, namely, the ratio of the EASA to the geometric area, is calculated to be 92.6. In contrast, the R_f value of an Au disc electrode is only 1.51. The EASA of the 3DMG electrode is 61 times that of Au disc electrode, and the high EASA of the 3DMG will be beneficial to the immobilization of Ab_1 and the capture of *S. aureus* cells.

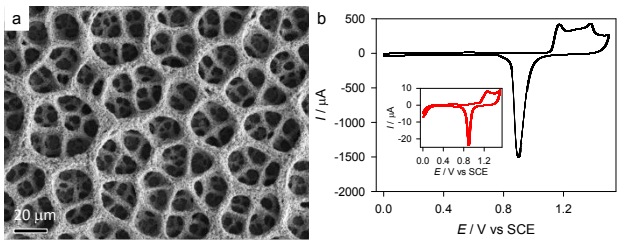

Fig. 1 (a) SEM image of 3DMG. (b) CVs of 3DMG and Au disk electrode (inset) in 0.5 M H_2SO_4 aqueous solution at 50 mV s^{-1}.

Characterizations and surface modifications of MSNs

The morphologies of MSNs were characterized by SEM (**Fig. 2a**) and transmission electron microscopy (TEM, **Fig. 2b**). The SEM image reveals that MSNs have uniform size (290±30 nm). TEM image further reveals that MSNs have porous structure. A hysteresis loop is observed in the nitrogen adsorption/desorption isotherms (**Fig. S1** †), indicating that mesopores exist in the MSNs. The Brunauer-Emmett-Teller surface area of the MSNs is as high as 1230 m^2 g^{-1}, and the average pore size is 3.7 nm according to Barret-Joyner-Halenda theory.

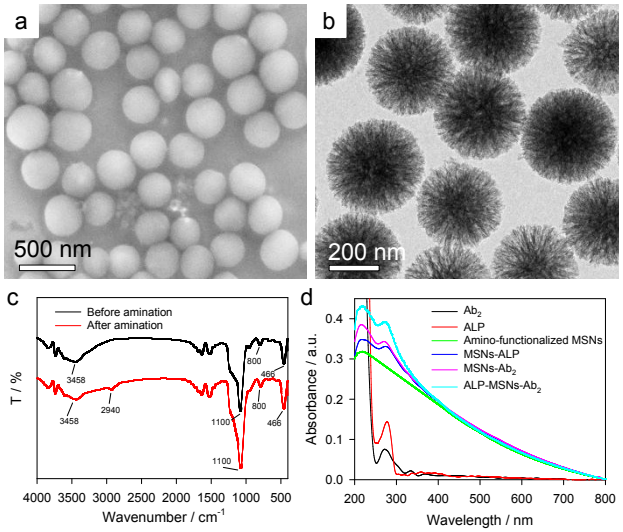

Fig. 2 (a, b) SEM (a) and TEM image (b) of MSNs. (c) FTIR spectra of MSNs before and after surface amination. (d) UV-Vis spectra of ALP, Ab_2, amino-functionalized MSNs, MSNs-ALP, MSNs-Ab_2, and ALP-MSNs-Ab_2.

For facile immobilization ALP and Ab_2, MSNs were subjected to surface amination by coating APTES on the surfaces of MSNs. In the Fourier transform infrared (FTIR) spectrum of MSNs (**Fig. 2c**), the sharp absorption peak at 1100 cm^{-1} and the small absorption peak at 800 cm^{-1} are due to the asymmetric and symmetric stretching vibration of Si-O bonds, respectively.[40] In addition, the sharp absorption peak at 466 cm^{-1} is resulting from the bending vibration of Si-O bonds, while the broad peak at 3458 cm^{-1} is resulting from the asymmetric stretching vibration of O-H.[41] After surface coating of APTES, a weak peak at 2940 cm^{-1} in the FTIR spectrum is assigned to the asymmetric stretching vibration of -CH_2 in the APTES. This result suggests that APTES was successfully modified on the surface of MSNs. Note here that the absorption peak of -NH_2 is overlapped with the absorption peak of -OH at 3458 cm^{-1}.

Amino-functionalized MSNs were used for the immobilization of ALP and Ab_2, and the product was studied by Ultraviolet-visible (UV-Vis) spectrometry. As shown in **Fig. 2d,** both ALP and anti-*S. aureus* Ab_2 show an absorption peak at 280 nm, which is a typical absorption peak of proteins.[42-44] Significant absorption peaks at 280 nm can also observed for MSNs-ALP, MSNs-Ab_2, and ALP-MSNs-Ab_2, indicating the successful immobilization of protein molecules on MSNs. However, the peak intensity at 280 nm of ALP-MSNs-Ab_2 is higher than those of MSNs-ALP and MSNs-Ab_2, indicating that more protein molecules are immobilized on MSNs. This result may indicate both ALP and Ab_2 were successfully linked to the surfaces of the MSNs.

Characterizations of immunoelectrodes

The fabrication steps of the immunoelectrodes are illustrated in **Scheme 1a**, and each fabrication step of the immunoelectrodes was

View Article Online
DOI: 10.1039/C9AN02000E

characterized by cyclic voltammetry (**Fig. 3a)** and electrochemical impedance spectroscopy (**Fig. 3b**). All the modification layers on 3DMG are non-conductive and have no redox activity, which will mainly affect the mass transfer of $[Fe(CN)_6]^{4-/3-}$. Thus all electrochemical impedance spectra were fitted to a simple equivalent circuit model. As shown in **Fig. 3a**, resulting from the redox of $[Fe(CN)_6]^{4-/3-}$, a pair of reversible redox peaks can be seen at the 3DMG electrode, and the redox peak separation (ΔE, E_{pa}-E_{pc}) is 85 mV. Based on the Randles equivalent circuit model, the charge transfer resistance (R_{ct}) is estimated to be 6 Ω for the 3DMG electrode (**Fig. 3b**). After the electrodeposition of CS on the 3DMG electrode, increased ΔE (90 mV) and R_{ct} (236 Ω) were obtained, indicating the successful modification of CS film on the 3DMG electrode. To specifically recognize *S. aureus* cells, Ab_1-CS/3DMG electrode was prepared, and further increased ΔE (119 mV) and R_{ct} (838Ω) were obtained. For blocking the nonspecific binding sites, BSA/Ab_1-CS/3DMG electrode was prepared, and the values of ΔE and R_{ct} are estimated to be 179 mV and 1667 Ω, respectively. The BSA/Ab_1-CS/3DMG electrode was used for capture of *S. aureus* cells (10^3 CFU mL^{-1}), and the values of ΔE and R_{ct} for the resulting *S. aureus*/BSA/Ab_1-CS/3DMG electrode are 220 mV and 2105 Ω, respectively. Finally, the *S. aureus*/BSA/Ab_1-CS/3DMG electrode was labeled with ALP-MSNs-Ab_2, and the values of ΔE and R_{ct} for the resulting ALP-MSNs-Ab_2/*S. aureus*/BSA/Ab_1-CS/3DMG electrode are 264 mV and 2735 Ω, respectively. One can see that each modification step can result in the increased ΔE and R_{ct}, confirming the successful preparation of the immunoelectrodes.

Fig. 3c and **d** show SEM images of the *S. aureus*/BSA/Ab_1-CS/3DMG electrode, and many *S. aureus* cells are observed on the electrode, confirming that *S. aureus* cells can be captured efficiently by the electrode. After being labeled with ALP-MSNs-Ab_2, one can see that many nanoparticles are linked to the *S. aureus* cell (**Fig. 3e**), suggesting that the ALP-MSNs-Ab_2 nanocomposites were successfully labeled to the *S. aureus* cell.

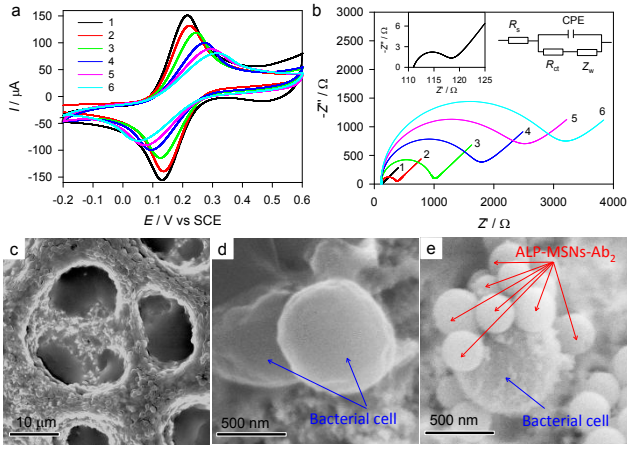

Fig. 3 CVs (a) at a scan rate of 50 mV s^{-1} and electrochemical impedance spectra (b) of 3DMG (1), CS/3DMG (2), Ab_1-CS/3DMG (3), BSA/Ab_1-CS/3DMG (4), *S. aureus*/BSA/Ab_1-CS/3DMG (5), ALP-MSNs-Ab_2/*S. aureus*/BSA/Ab_1-CS/3DMG (6) in 0.10 M PBS (pH 7.4) containing 5.0 mM $K_3Fe(CN)_6$ and 5.0 mM $K_4Fe(CN)_6$. Inset of b shows electrochemical impedance spectrum of 3DMG and equivalent circuit model. Electrochemical impedance spectra were obtained in the frequency range from 1 MHz to 0.01 Hz at voltage amplitude of 5 mV. SEM images of *S. aureus*/BSA/Ab_1-CS/3DMG (c, d) and ALP-MSNs-Ab_2/*S. aureus*/BSA/Ab_1-CS/3DMG (e).

Electrochemical detection of *S. aureus*

The ALP-MSNs-Ab_2/*S. aureus*/BSA/Ab_1-CS/3DMG electrodes were subjected to ALP-catalyzed silver deposition. As shown in **Scheme 1b**, due to the catalysis of ALP, AAP can be converted to ascorbic acid (AA), and then AA can react with $AgNO_3$ and Ag will deposit on the immunoelectrodes.[45, 46] The deposited Ag on the immunoelectrodes was converted to Ag(I) ions by HNO_3 leaching, and then differential pulse voltammetric detection was carried out to quantitatively detect *S. aureus*.

To achieve the highest detection signal, various experimental conditions for the preparation of the immunoelectrodes were optimized (**Fig. S2** †). The optimal incubation time for *S. aureus* capture is 80 min, and the optimal incubation time for ALP-MSNs-Ab_2 labeling is 45 min. Experimental conditions for ALP-catalyzed silver deposition were also optimized (**Fig. S3** †). The optimal $AgNO_3$ concentration is 3 mM, the optimal AAP concentration is 3.5 mM, and the optimal reaction time for ALP-catalyzed silver deposition is 45 min. Experimental conditions for differential pulse voltammetric detection were also optimized (**Fig. S4** †). The optimal deposition potential is -0.3 V**,** and the optimal deposition time is 200 s.

Under these optimized experimental conditions, *S. aureus* was quantitatively detected by differential pulse voltammetry (**Fig. 4a**). The peak current (I_P, mA) in DPVs increases accordingly with the increase of *S. aureus* concentration (c, CFU mL^{-1}). **Fig. 4b** shows the calibration curve for detecting *S. aureus* using the 3DMG-based immunobiosensor, which shows a good linear relationship from 5 to 10^9 CFU mL^{-1}. The linear fitting curve equation is $I_p = 0.139 \log c - 0.122$ ($R^2 = 0.9987$). The relative standard deviation (RSD) for three parallel tests was below 5%. The detection limit of the 3DMG-based immunobiosensor is 2 CFU mL^{-1} (S/N=3). A biosensor was also constructed on a gold disc electrode, and the fabrication steps of the Au disk electrode-based biosensor were similar to those of the 3DMG-based biosensor except that the Au disk electrode was used instead of the 3DMG electrode. As shown in **Fig. 4c** and **d**, the Au disk electrode-based biosensor shows a linear range from 50 to 10^8 CFU mL^{-1}. The linear fitting curve equation is I_p=0.0150 log$c$-0.0255 (R^2 = 0.9948). The detection limit of the Au disk electrode-based biosensor is evaluated to be 20 CFU mL^{-1} (S/N=3). Obviously, the detection limit of the 3DMG-based biosensor is much lower than that of the Au disk electrode-based biosensor. Foodborne pathogenic bacteria usually exist in real samples in very low numbers (<20 CFU mL^{-1}),[15] so the detection limit of the Au disk electrode-based biosensor is still not up to the application requirements. The 3DMG-based biosensor can detect *S. aureus* down to 2 CFU mL^{-1}, which can meet the practical application requirements. Also, the sensitivity of the 3DMG -based biosensor (0.139 mA CFU^{-1} mL) is 9 times that of the Au disk electrode-based biosensor (0.0150 mA CFU^{-1} mL), suggesting that the 3DMG electrode can amplify the detection signal. The 3DMG has a high surface area and abundant macropore (20 - 50 μm), and these features are beneficial to the immobilization of Ab_1 and the capture of *S. aureus*. At the same *S. aureus* concentration,

View Article Online
DOI: 10.1039/D0AN02325E

the 3DMG can capture more *S. aureus* than the Au disk electrode. In our work, the ALP-MSNs-Ab_2 composites were labeled to the captured *S. aureus* cells. Compared with the Au disk electrode-based immunoelectrode, more Ag will deposit on the 3DMG-based immunoelectrode after the ALP-catalyzed silver deposition, thus resulting in higher differential pulse voltammetric signal. Moreover, the detection limit of the 3DMG-based immunobiosensor is lower than those of most electrochemical biosensors in literature, and only a little higher than that of an electrochemical sandwich aptasensor (**Table S1**).[47] In this work, the electrochemical signal of the 3DMG-based immunobiosensor was amplified by effectively integrating sensitive electrochemical detection with enzymatic amplification and 3DMG-assisted signal-amplification, so the proposed method is sensitive than the reported electrochemiluminescence, colorimetry, surface-enhanced Ranman scatting, fluorescence, and polymerase chain reaction in literature (**Table S1**). Although label-free biosensors based on electrochemical impedance technique can be used to directly detect pathogenic bacteria, the detection limits are typically higher than 100 CFU mL^{-1}.[48, 49] Although the fabrication steps of the biosensor are somewhat complex, the proposed biosensor may still have a great application prospect in the detection of pathogenic bacteria due to its high sensitivity.

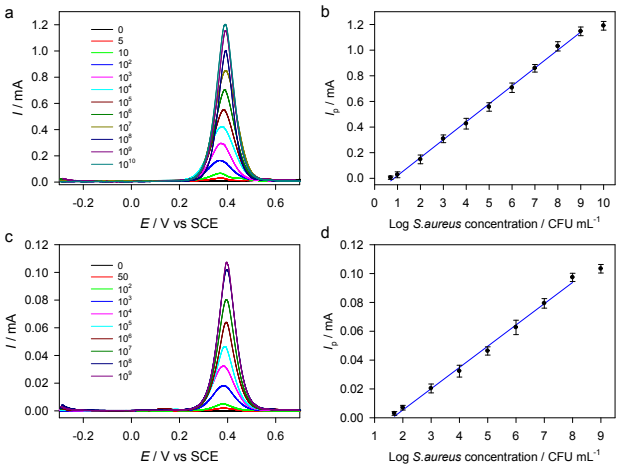

Fig. 4 DPVs (a) and standard curve (b) for *S. aureus* detection using 3DMG-based biosensor. DPVs (c) and standard curve (d) for *S. aureus* detection using Au disk electrode-based biosensor. Error bars represent the standard deviation.

The selectivity of both the 3DMG-based biosensor and the Au disk electrode-based biosensor was tested. As shown in **Fig. 5** and **Fig. S5** †, both the 3DMG-based biosensor and the Au disk electrode-based biosensor have good selectivity toward *S. aureus* detection. The specific affinity of *anti-S. aureus* antibodies is mainly responsible for the selectivity toward *S. aureus* detection, so there was no significant difference in selectivity between the 3DMG-based biosensor and the Au disk electrode-based biosensor. To study the reproducibility of the biosensor, 6 immunoelectrodes were prepared under the same conditions, and the detection of *S. aureus* (10^3 CFU mL^{-1}) using an immunoelectrode was carried out every 3 day (**Fig. S6a** †). The relative standard deviations are below 5.5%, suggesting the proposed immunoelectrodes have excellent reproducibility. We also detect *S. aureus* in milk samples using the 3DMG-based biosensor and the Au disk electrode-based biosensor (**Table S2**). As shown in **Table S2** †, the detection of *S. aureus* using the Au disk electrode-based biosensor at a low concentration of 10 CFU mL^{-1} is infeasible, resulting from the relative high detection limit (20 CFU mL^{-1}). In contrast, the 3DMG-based biosensor can still show satisfactory recovery for detecting *S. aureus* at a low concentration of 10 CFU mL^{-1}, highlighting the advantage of the 3DMG-based biosensor. Foodborne pathogenic bacteria usually exist in real samples in very low numbers (<20 CFU mL^{-1}),[15] so so the 3DMG-based biosensor is more suitable for the detection of foodborne pathogenic bacteria in real samples than the Au disk electrode-based biosensor. To further validate for detection of *S. aureus* in milk samples using the 3DMG-based biosensor, we also detected *S. aureus* in milk samples using our reported method that combines immunomagnetic separation with fluorescent immunoassay.[11] As shown in **Table S3** †, the results obtained by the 3DMG-based biosensor are in good agreement with those obtained by the fluorescent immunoassay, confirming that our method can be used to detect *S. aureus* in real samples.

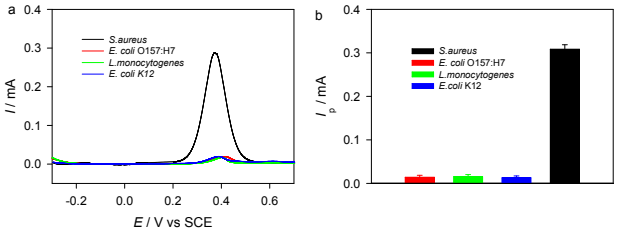

Fig. 5 DPVs (a) and peak currents (b) for detecting different pathogens using 3DMG-based biosensor. The concentrations of all pathogens are 10^3 CFU mL^{-1}. Error bars represent the standard deviation.

4. Conclusions

In summary, 3DMG electrode was prepared by the dynamic hydrogen bubble template method, and used to construct an electrochemical immunobiosensor for detecting *S. aureus*. ALP-loaded MSNs served as signal tags to construct a sandwich-type electrochemical immunobiosensor. Based on the alkaline phosphatase-catalyzed silver deposition and differential pulse voltammetric detection, the immunobiosensor can detect *S. aureus* down to 2 CFU mL^{-1}. Because the macroporous structure of the 3DMG electrode is beneficial to the immobilization of Ab_1 and the capture of *S. aureus*, the sensitivity of the 3DMG-based immunobiosensor is 9 times that of the Au disk electrode-based immunobiosensor. The immunobiosensor also has excellent selectivity, high stability and good reproducibility. The immunobiosensor can also be used for detecting *S. aureus* in milk samples. We believe that the 3DMG electrode can also be used for the construction other biosensors for signal-amplification detection of other targets.

Conflicts of interest

There are no conflicts to declare.

View Article Online
DOI: 10.1039/C9AN02393F

Acknowledgements

This work was supported by the NNSF of China (21705045, 21675050, and 21775041), the NSF of Hunan Province (2018JJ2252), the Science and Technology Innovation Project of Hunan Province (2018RS3062), and the Science and Technology Project of Changsha (KQ1905028).

Notes and references

1. A. K. Deisingh and M. Thompson, *J. Appl. Microbiol.*, 2004, **96**, 419-429.
2. P. K. Mandal, A. K. Biswas, K. Choi and U. K. Pal, *Am. J. Food Tech.*, 2011, **6**, 87-102.
3. Y. Zeng, Y. Wan and D. Zhang, *Microchim. Acta*, 2016, **183**, 741-748.
4. S. Lim, D. H. Lee, W. Kwak, H. Shin, H. J. Ku, J. e. Lee, G. E. Lee, H. Kim, S. H. Choi, S. Ryu and J. H. Lee, *J. Microbiol. Biotechnol.*, 2015, **25**, 98-108.
5. W. Chunglok, D. K. Wuragil, S. Oaew, M. Somasundrum and W. Surareungchai, *Biosens. Bioelectron.*, 2011, **26**, 3584-3589.
6. J. Lee, C. Park, Y. Kim and S. Park, *BioChip J.*, 2017, **11**, 287-293.
7. R. Wu, Y. Ma, J. Pan, S.-H. Lee, J. Liu, H. Zhu, R. Gu, K. J. Shea and G. Pan, *Biosens. Bioelectron.*, 2018, **101**, 52-59.
8. H. Shen, J. Wang, H. Liu, Z. Li, F. Jiang, F.-B. Wang and Q. Yuan, *ACS Appl. Mater. Interfaces*, 2016, **8**, 19371-19378.
9. M. Majdinasab, A. Hayat and J. L. Marty, *Trends Anal. Chem.*, 2018, **107**, 60-77.
10. S. Wang, W. Deng, L. Yang, Y. Tan, Q. Xie and S. Yao, *ACS Appl. Mater. Interfaces*, 2017, **9**, 24440-24445.
11. W. Deng, C. Cheng, H. Yang, H. Wang, Y. Tan, Q. Xie, M. Ma and S. Yao, *Talanta*, 2019, **202**, 244-250.
12. A. Abbaspour, F. Norouz-Sarvestani, A. Noori and N. Soltani, *Biosens. Bioelectron.*, 2015, **68**, 149-155.
13. X. Liao, H. Fu, T. Yan and J. Lei, *Biosens. Bioelectron.*, 2019, **146**, 111743-111743.
14. M. Zhong, L. Yang, H. Yang, C. Cheng, W. Deng, Y. Tan, Q. Xie and S. Yao, *Biosens. Bioelectron.*, 2019, **126**, 493-500.
15. V. Velusamy, K. Arshak, O. Korostynska, K. Oliwa and C. Adley, *Biotechnol. Adv.*, 2010, **28**, 232-254.
16. F. S. Ke, L. Huang, H. H. Jiang, H. B. Wei, F. Z. Yang and S. G. Sun, *Electrochem. Commun.*, 2007, **9.**, 228-232.
17. G. Lui, G. Li, X. Wang, G. Jiang, E. Lin, M. Fowler, A. Yu and Z. Chen, *Nano Energy*, 2016, **24**, 72-77.
18. Y. Chen, Y. Zhu and Z. Chen, *Thin Solid Films*, 2013, **539**, 122-126.
19. W. Deng, Y. Zhang, Y. Tan and M. Ma, *J. Electroanal. Chem.*, 2017, **787**, 103-109.
20. Y. Li, X. Wang and M. Cao, *J. CO2 Util.*, 2018, **27**, 204-216.
21. G. B. Darband, M. Aliofkhazraei, A. S. Rouhaghdam and M. A. Kiani, *Appl. Surf. Sci.*, 2019, **465**, 846-862.
22. B. Murugesan, N. Pandiyan, M. Arumugam, M. Veerasingam, J. Sonamuthu, A. R. Jeyaraman, S. Samayanan and S. Mahalingam, *Carbon*, 2019, **151**, 53-67.
23. S. Peng, H. Jiang, Y. Zhang, L. Yang, S. Wang, W. Deng and Y. Tan, *J. Mater. Chem. A*, 2016, **4**, 3678-3682.
24. Y. Zhang, M. Chu, L. Yang, W. Deng, Y. Tan, M. Ma and Q. Xie, *Chem. Commun.*, 2014, **50**, 6382-6385.
25. L. Yang, Y. Zhang, M. Chu, W. Deng, Y. Tan, M. Ma, X. Su, Q. Xie and S. Yao, *Biosens. Bioelectron.*, 2014, **52**, 105-110.
26. Y. Zhao, F. Dong, W. Han, H. Zhao and Z. Tang, *Micropor. Mesopor. Mater.*, 2019, **273**, 1-9.
27. H. Jiang, L. Yang, W. Deng, Y. Tan and Q. Xie, *J. Power Sources*, 2017, **363**, 27-33.
28. L. Yang, S. Wang, S. Peng, H. Jiang, Y. Zhang, W. Deng, Y. Tan, M. Ma and Q. Xie, *Chem. Eur. J.*, 2015, **21**, 10634-10638.
29. S. You, M. Ma, W. Wang, D. Qi, X. Chen, J. Qu and N. Ren, *Adv. Energy Mater.*, 2017, **7**, 1601364.
30. Y. Zhang, M. Chu, L. Yang, Y. Tan, W. Deng, M. Ma, X. Su and Q. Xie, *ACS Appl. Mater. Interfaces*, 2014, **6**, 12808-12814.
31. Y. Wang, M. Cui, M. Jiao and X. Luo, *Anal. Bioanal. Chem.*, 2018, **410**, 5871-5878.
32. J. H. Shim, A. Cha, Y. Lee and C. Lee, *Electroanalysis*, 2011, **23**, 2057-2062.
33. W. Deng, X. Yuan, Y. Tan, M. Ma and Q. Xie, *Biosens. Bioelectron.*, 2016, **85**, 618-624.
34. J. Liu, L. Cao, W. Huang and Z. Li, *ACS Appl. Mater. Interfaces*, 2011, **3**, 3552-3558.
35. L. Zhang, W. He, J. Yang, J. Sun, H. Li, B. Han, S. Zhao, Y. Shi, Y. Feng, Z. Tang and S. Liu, *Biosens. Bioelectron.*, 2018, **122**, 217-223.
36. Q. Zhou, Q. Xie, Y. Fu, Z. Su, X. e. Jia and S. Yao, *J. Phys. Chem. B*, 2007, **111**, 11276-11284.
37. H. Angerstein-Kozlowska, B. E. Conway, A. Hamelin and L. Stoicoviciu, *Electrochim. Acta*, 1986, **31**, 1051-1061.
38. Y. Lee, A. Loew and S. Sun, *Chem. Mater.*, 2010, **22**, 755-761.
39. A. Devadoss, H. Han, T. Song, Y.-P. Kim and U. Paik, *Analyst*, 2013, **138**, 5025-5030.
40. S. Ishizuka, S. Kato, Y. Okamoto and K. Akimoto, *Appl. Phys. Lett.*, 2002, **80**, 950-952.
41. H. Xue, J. Zhao, Q. Zhou, D. Pan, Y. Zhang, Y. Zhang and Y. Shen, *ACS Appl. Nano Mater.*, 2019, **2**, 1579-1588.
42. B. Sun, J. Dong, L. Cui, T. Feng, J. Zhu, X. Liu and S. Ai, *Biosens. Bioelectron.*, 2019, **124**, 1-7.
43. H. Dong, T.-T. Han, L.-L. Ren and S.-N. Ding, *J. Electroanal. Chem.*, 2017, **806**, 32-40.
44. G.-C. Fan, L. Han, H. Zhu, J.-R. Zhang and J.-J. Zhu, *Anal. Chem.*, 2014, **86**, 12398-12405.
45. J. Wei, W. Chang, A. Qileng, W. Liu, Y. Zhang, S. Rong, H. Lei and Y. Liu, *Anal. Chem.*, 2018, **90**, 9606-9613.
46. A. Xu, L. Chao, H. Xiao, Y. Sui, J. Liu, Q. Xie and S. Yao, *Biosens. Bioelectron.*, 2018, **104**, 95-101.
47. A. Abbaspour, F. Norouz-Sarvestani and A. N. a. N. Soltani, *Biosens. Bioelectron.,* , 2015, **68**, 149-155.

View Article Online
DOI: 10.1039/C9AN02392E

48. R. D. Das, A. Dey, S. Das and C. RoyChaudhuri, *IEEE Sens. J.*, 2010, **11**, 1242-1252.
49. N. Pal, S. Sharma and S. Gupta, *Biosens. Bioelectron.*, 2016, **77**, 270-276.

View Article Online
DOI: 10.1039/C9AN02392E

Table of Contents

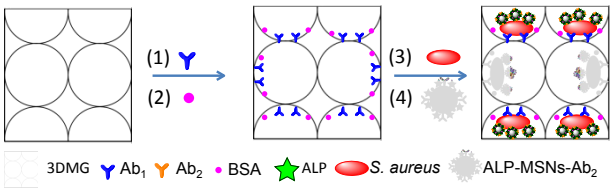

Three-dimensional macroporous gold is superior to conventional gold disk electrode in the construction of electrochemical immunobiosensor for *Staphylococcus aureus* detection.